Langevin Rigid: Animating Immersed Rigid Bodies in Real-time

Haoran Xie **Kazunori Miyata**

Japan Advanced Institute of Science and Technology

{xiehr, miyata}@jaist.ac.jp

Abstract

We present the *Langevin rigid* approach, a technique for animating the dynamics of immersed rigid bodies in viscous incompressible fluid in real-time. We use generalized Kirchhoff equations to ensure forces and torques from the surrounding fluid that create realistic motion of immersed rigid bodies. We call our method the *Langevin rigid* approach because the generalized Langevin equations are applied to represent the effects of turbulent flow generated at the body surface. The Langevin rigid approach precomputes added-mass effects and the vortical loads from turbulent model, and executes the rigid body solver in runtime, so that this method is straightforward and efficient to the interactive simulations. Many types of rigid bodies with lightweight mass (e.g. leaf or paper) can be simulated realistically in high-Reynolds-number flows.

Keywords: rigid body dynamics, generalized Langevin equations, generalized Kirchhoff equations, turbulence

1 Introduction

Rigid body simulations are the fundamental techniques in computer animation, which are ubiquitously used in various applications. The rigid bodies sometimes easily fluctuate while falling through a fluid (e.g. water or air) in reality, especially for the lightweight objects. It is a challenging and promising issue to handle the dynamics of immersed rigid bodies, because the phenomena are common in daily life and can enhance the reality of simulations.

The motion of immersed rigid body is characterized by a Reynolds number Re and the mean falling velocity U_0.

$$Re = \frac{U_0 d}{\nu}; \qquad U_0 = \sqrt{(\bar{\rho} - 1)gb} \tag{1}$$

where ν is the kinematic viscosity of the surrounding fluid; d and b are the characteristic length and thickness of the rigid body; and $\bar{\rho}$ is the body-to-fluid density ratio. For a common leaf, the Reynolds number would be at the magnitude of 10^4. For a high-Reynolds-number flow, the turbulence is generated around the body and then detached from the body surface as vortex shedding. The motion of the body becomes unsteady and shows a chaotic trajectory.

Two-way coupling between rigid bodies and incompressible fluid focuses on the motions of both fluid and rigid, which requires heavy computation to resolve Navier-Stokes equations in an Eulerian or Langrangian way. The simulation of immersed rigid bodies concerns about the realistic motions of the body. Unlike one-way fluid-solid coupling, the interaction from the surrounding flow plays a significant role in the dynamics of the immersed body. In this paper, we propose the Langevin rigid approach as a tradeoff between two-way and one-way coupling schemes to resolve the dynamics of immersed rigid bodies.

Our precomputation step captures the characteristics of the turbulent flow generated around the object, and stores the turbulent energy and its dissipation rate for obtaining vortical loads on the body. The vortical loads are represented in the Langevin equation as a stochastic process of the object velocity. We also precompute the added-mass tensors due to both translational and rotational displacements of the surrounding flow. Our approach only runs a rigid body solver in runtime to solve the ordinary differential equations originated from Kirchhoff.

Overall, our approach allows us to efficiently simulate immersed rigid bodies with arbitrary shapes in low computation cost. An overview of our approach

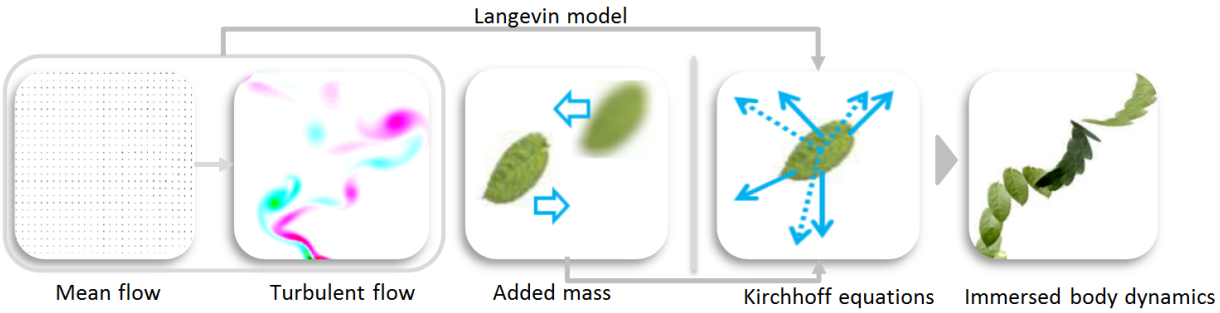

Figure 1: An overview of different steps of our approach. The pre-computation steps include a turbulent model based on its mean flow and the calculation of added-mass tensors. After precomputing the external forces and torques, the generalized Kirchhoff equations is solved in runtime. The final result is the creation of the dynamics of an immersed rigid body.

is illustrated in Figure 1. The major contributions of this work are as follows:

- A new method based on generalized Langevin equations of both translational and rotational velocities to represent the characteristics of the surrounding flow.
- A new representation of rigid body dynamics as generalized Kirchhoff equation in body-fixed frame to account for all external forces and torques.
- An algorithm to process the precomputed data from both added-mass effects and the k-ε turbulent model.

The rest of this paper is organized as follows: Section 2 highlights the related work in two-way coupling between solid and fluid. Section 3 details the equations of rigid body by the Kirchhoff equations. Section 4 explains the Langevin model to capture the motion in a stochastic process way, and Section 5 gives the approach on how to obtain turbulent parameters in the k-ε turbulent model. Section 6 describes the algorithms used in the implementation of our approach. Section 7 shows the simulation results of different objects by our approach. Finally, we conclude this paper with a discussion of possible future work in Section 8.

2 Related Work

Two-way coupling between rigid body and incompressible fluid has been studied extensively in computer graphics. Basically there are two types of schemes on this research. The first scheme handles fluid in Euler formulation and rigid bodies in Lagrangian formation [4, 9, 1, 6]. Guendelman et al.[9] proposed a robust ray casting algorithm for the coupling between fluid and cloths to avoid fluid leaking. Carlson et al. [4] treated the rigid body as fluid grid by using distributed Langrange multiplier. The second scheme is the fully Langrangian meshless method [7, 18, 2]. Becker et al. [2] proposed a direct forcing method in a predictor-corrector scheme with SPH particles. Solenthaler et al. [18] used a penalty method to analyze the forces on the immersed boundary. All these methods focus on the motion of the surrounding fluids and requires high computation cost.

The work [21] introduced a Kirchhoff tensor to represent added-mass effects for underwater rigid body simulations. This approach is only suitable for the inviscid and irrotational flow with low Reynolds number, because the drag effects in this approach were chosen to be linearly related to the body velocity. In this paper, we propose a Langevin model related to the turbulent flow for solving the vortical loads.

Langevin equations describe the Browian motion of suspended bodies in flow. Recently Zhao et al. [5, 23] applied the Langevin model to enhance turbulent flow simulation and the floating lightweight rigid body. In these papers, the rotational velocity and the coupling between translational and rotational velocities are not considered. We resolve these issues by combing Kirchhoff equations with Langevin model in this paper.

3 Equations of Motion

Let us consider a rigid body of mass m, and center of mass O moving through an incompressible fluid with density ρ_f. The motion of the rigid body is described by $(R(t), x(t))$. The $R(t)$ describes the orientation of the body as a 3×3 orthogonal matrix rather than a quaternion form, and $x(t)$ is the position of O in the

inertial reference frame at time step t. We will define the equations of motion in a body-fixed frame.

3.1 Kinematic Equation

The translational and angular velocities of the object $(\omega, v) \in R^6$ are given in body-fixed frame as follows:

$$\dot{R} = R\hat{\omega}, \qquad \dot{x} = Rv \tag{2}$$

where $R\hat{\omega} = R \times \omega$, and $\hat{\omega}$ is defined as

$$\begin{pmatrix} 0 & -\omega(3) & \omega(2) \\ \omega(3) & 0 & -\omega(1) \\ -\omega(2) & \omega(1) & 0 \end{pmatrix} \tag{3}$$

where $\omega(n)$ is the n-th element of angular velocity ω.

3.2 Dynamic Equation

The dynamics of a rigid body immersed in a viscous fluid results from the coupling between the body and the surrounding flow. The dynamical effects from the interaction of the fluid to a body displacement, including both translational and rotational transformations, are described as added-mass tensors M_f and J_f. M_f represents the force and torque due to the fluid coupling to a translational acceleration of the body and J_f is to a rotational acceleration. Therefore, the dynamics is governed by the generalized Kirchhoff equations [8]. The dynamic equation has the following form in the body-fixed frame.

$$\begin{aligned} M \cdot \dot{v} + v \times (M \cdot \omega) &= F_t + F_g \\ J \cdot \dot{\omega} + \omega \times (J \cdot \omega) + v \times (M_f \cdot v) &= \Gamma_t + \Gamma_g \end{aligned} \tag{4}$$

where $M = mI + M_f$, $J = J_0 + J_f$, J_0 is the moment of inertia of the body and I is the 3×3 identity matrix. F_t and Γ_t are the resulted force and torque due to the turbulence generated at the body surface while the body moves in a viscous flow; F_g and Γ_g result from the buoyancy-corrected gravity.

Because the added-mass tensors M_f and J_f are only determined by the body geometry and not affected by the generated turbulence at body surface [10], M_f and J_f can be computed in a precomputation step.

3.2.1 Precomputaion of Added-mass Tensors

The traditional way to compute added-mass tensors directly integrates the potential pressure over the body surface with a constant acceleration in an inviscid, incompressible flow [3]. We use a precomputation strategy similar to [21] for calculating added-mass tensors. Comparing with other approaches, this method is straightforward and plausible in CG literature. As in [21], the added-mass tensors are directly given as follows:

$$\nabla\cdot\langle u\rangle = 0\frac{1}{\rho}\nabla P+\nabla\cdot(\nu+v_T)(\nabla\langle u\rangle+\nabla^T\langle u\rangle)\frac{\partial(\nabla\phi(p_i)-(\omega\times p_i+v}{\partial n} \tag{5}$$

where p_i is the center of facet Γ_i on the boundary of the immersed body; and $n(p)$ is the normal vector at the boundary point p; and σ_j is the strength at source position s_j, which is given as follows:

$$\sigma = M^{-1}\sum_i \langle \omega \times p_i + v, n(p_i)\rangle vol(\Gamma_i) \tag{6}$$

M is a matrix of solid angles subtended by facets and the sum term in Eq.(6) describes the normal flux through facets calculated using the approximation in [20].

The source position s_j is obtained by taking an offset n to the vertex positions on the body surface. For thin objects, such as leaves and papers, we make sure that $n \ll l$ the thickness of the body. In our work, we chose the rate n/l as 0.2.

3.2.2 Buoyancy-corrected Gravity

Both the gravity and buoyancy forces are applied to the immersed rigid body whose directions are inverse. We express them in body-fixed frame as follows:

$$F_g = R^T(m - \rho_f V)g \tag{7}$$

$$\Gamma_g = \rho_f V\vec{r} \times R^T g \tag{8}$$

where V is the volume of the body and vector $\vec{r}$ is from the center of mass to the center of buoyancy in body-fixed frame.

The difficulty of solving Eq.(4) is how to determine the force F_t and torque Γ_t due to surrounding turbulent flow, which cause path instability of the body in a chaotic way. We will describe the approach to add vortical loads (force and torque) in the next section.

4 Langevin Model

The stochastic model for the motion of suspended fluid particles is proposed by Langevin decades ago. According to this model, the velocity increments in continuous time steps are highly correlated, which is called the Ornstein-Unlebeck process [19]. The model can be applied to describe the Brownian motion of lightweight objects undergoing the vortical loads from the surrounding turbulent flow [13][23].

For a statistically isotopic turbulence, the Langevin equation can be defined as following stochastic differential equation:

$$du(t) = -\alpha u(t)dt + \beta dW \tag{9}$$

where $u(t)$ is the translational velocity of the fluid particle; α and β are the relaxation rate and the diffusion coefficient, which reveal the properties of the turbulent flow; and W is a Wiener process, which represents a Brownian motion with a continuous-time stochastic process. In the implementation, the process is calculated by a normal distribution with mean of zero and variance of the time interval Δt.

For a fluid particle with arbitrary shape, the relaxation term in Eq.(9) has no effect to angular velocity increments of the body as a rotational Brownian motion [13]. The Langevin equation for angular velocity is given as:

$$d\omega(t) = \beta dW \tag{10}$$

4.1 Generalized Langevin Equation

Pope [16] described the generalized Langevin equation for the suspended particle in a turbulent flow. The equation gives the expressions of α and β having the following forms:

$$\alpha = (\frac{1}{2} + \frac{3}{4}C_0)\frac{\varepsilon}{k}, \qquad \beta = (C_0\varepsilon)^{\frac{1}{2}} \tag{11}$$

where k and ε are kinetic energy and its dissipation rate of the surrounding turbulent flow; C_0 is a Kolmogorov coefficient. According to the Kolmogorov hypothesis, C_0 is related to the Reynolds number Re of the flow [17].

$$C_0(Re) = 6.5(1 + 140Re^{-\frac{4}{3}})^{-\frac{3}{4}} \tag{12}$$

For high-Reynolds-number flow ($Re > 10^3$), this relation is empirically fitted.

Finally, the dynamic equations of immersed body are discretized through finite-difference scheme by substituting Eqs.(9)(10)(11) into Eq.(4).

$$\begin{aligned} v(t+\Delta t) - v(t) = M^{-1}(&-v(t) \times (M\omega(t))\Delta t \\ &-\chi(\tfrac{1}{2} + \tfrac{3}{4}C_0)\Delta t \\ &+(C_0\varepsilon\Delta t)^{\frac{1}{2}}\vec{\xi_1} + F_g(t)\Delta t) \end{aligned} \tag{13}$$

$$\begin{aligned} \omega(t+\Delta t) - \omega(t) = J^{-1}(&-\omega(t) \times (J\omega(t))\Delta t \\ &-v(t) \times (M_f v(t))\Delta t \\ &+(C_0\varepsilon\Delta t)^{\frac{1}{2}}\vec{\xi_2} + \Gamma_g(t)\Delta t) \end{aligned} \tag{14}$$

where $\chi = \varepsilon/k$;$\vec{\xi_1}$ and $\vec{\xi_2}$ are the vectors of normal Gaussian distributed variables with mean zero and unit deviation as $Norm(0, 1)$. The vectors are generated using the Box-Muller algorithm in our work.

The parameters (χ, ε) measure the characteristics of the surrounding turbulent flow. We pre-generate these parameters $(\chi(t), \varepsilon(t))$ by two-equation k-ε model in the next section.

5 Turbulence Model

In a turbulent flow, the fluid velocity u can be represented by Reynolds decomposition with the mean flow $\langle u \rangle$ and fluctuating velocity u' ($u = \langle u \rangle + u'$). The common approach for solving the fluid-rigid coupling problem based on the three dimensional Navier-Stokes equations are extremely computationally expensive, because the fluctuations of turbulence would be of small scale and high frequency. It is obvious not suitable for an interactive application. The most widely used turbulence model is the k-ε turbulent model by [12], which requires low computational cost. The k-ε model is a semi-empirical model based on the transport equations, which consist of two coupled equations for the turbulent kinetic energy k and its dissipation rate ε. The energy transport equations are defined as follows:

$$\begin{aligned} D_t k &= \nabla \cdot ((\nu + \tfrac{v_T}{\sigma_k})\nabla k) + G - \varepsilon \\ D_t \varepsilon &= \nabla \cdot ((\nu + \tfrac{v_T}{\sigma_\varepsilon})\nabla \varepsilon) + \chi(C_1 G - C_2 \varepsilon) \end{aligned} \tag{15}$$

where σ_k and σ_ε are the turbulent Prandtl numbers for k and ε; C_1 and C_2 are empirical constants. The empirical values are given as: $\sigma_k = 1.0$, $\sigma_\varepsilon = 1.3$, $C_1 = 1.44$ and $C_2 = 1.92$ [12].

The turbulent viscosity v_T describes the small scale turbulent motion as a viscous diffusion scale in the turbulent model. Turbulent viscosity v_T is defined as:

$$v_T = C_\mu \frac{k^2}{\varepsilon} \tag{16}$$

where $C_\mu = 0.09$ is an empirical constant.

The term G represents the generation of turbulent kinetic energy due to the mean velocity gradients and can be defined in terms of the strain tensor of the flow:

$$G = 2v_T \sum_{ij} S_{ij}^2 \tag{17}$$

where $S_{ij} = \frac{1}{2}(\frac{\partial \langle u \rangle_i}{\partial x_j} + \frac{\partial \langle u \rangle_j}{\partial x_i})$.

In the implementation, we simplify Eq.(15) by avoiding the incorporating diffusion terms in these equations, which are proven to be visually unnecessary in [14]. The following equations are used to represent transport equations:

$$D_t k = G - \varepsilon \tag{18}$$

$$D_t \varepsilon = \chi(C_1 G - C_2 \varepsilon) \tag{19}$$

In cases of high turbulent flows with high Reynolds numbers, the initial state (k_0, ε_0) is defined in terms of the mean falling velocity U_0 (Eq.1) which is used to estimate the information about the history of the moving body. The initial conditions for energy transport equations are given as follows:

$$k_0 = \frac{3}{2}U_0^2; \qquad \varepsilon_0 = \frac{C_\mu^{\frac{3}{4}} k_0^{\frac{3}{2}}}{l} \tag{20}$$

where l is the length scale of the MAC grid cell in the base flow simulation.

The turbulent parameters (χ, ε) are explicitly solved with finite difference scheme from Eqs.(18), (19) and (17) as shown in Figure 2, where a standard fluid solver is applied to obtain the mean velocities $\langle u \rangle$ of the base flow. According to the Kolmogorov theory, for high Reynolds number, the initial turbulence is unstable and the kinetic energy is divided into smaller scales. After reaching a critical scale value, turbulent energy dissipates due to viscosity, creating an energy cascade [15]. Figure 2 shows the varying dissipate rate accompanying the kinetic energy in our calculated result.

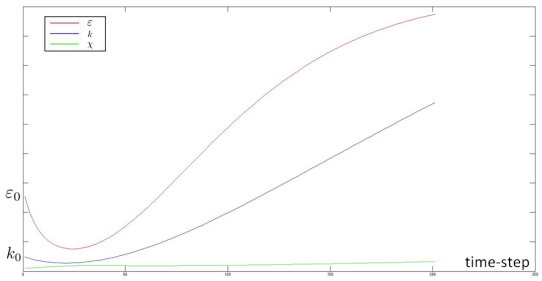

Figure 2: Turbulent parameters (χ, ε) at time steps with $Re = 3.8 \times 10^3$ and $32 \times 32 \times 16$ MAC grids.

6 Implementation

The implementation of our approach consists of two computation phases: pre-computations of added-mass tensors and turbulent flow; and runtime simulation of a rigid body solver. The calculation of added-mass tensors was described in Section 3.2.1.

Turbulent flow The turbulent model is based on a standard fluid solver to resolve the mean flow around the body. However, the complicated solver of Reynolds-averaged Navier-Stokes equations is usually applied to the k-ε model for accurate solutions, the standard solver can be more visually plausible and efficient in CG [15].

We apply a typical MAC staggered grid with semi-Langragian advection to obtain the base mean flow as described in Algorithm 1. The inflow velocity is chosen as the mean falling velocity (Eq.(1)) and defined as:

$$U_{in} = U_0 \tag{21}$$

Algorithm 1 Pseudo-code for pre-generated turbulent model.

```
Boundary conditions ←Eqs.(20)(21)
Timestep t = 0
while not stopped do
    // solve the mean flow ⟨u⟩
    Convection by semi-Langrangian
    Pressure projection by Poisson solver

    // Energy transport
    Compute turbulent viscosity v_T ←Eq.(16)
    Compute strain tensor term G ←Eq.(17)
    Integrate turbulent energy k ←Eq.(18)
    Integrate dissipation rate ε ←Eq.(19)

    t = t + Δt
end while
Output: (χ, ε)
```

Rigid body solver Our Langevin rigid approach is relatively efficient for real-time simulations, because the computation burdens involving turbulent flow effects are executed in pre-computation steps. The most runtime computation is for the rigid body solver, which is described in Algorithm 2. We apply a standard Runge-Kutta scheme for resolving the coupling dynamic equations, Eq.(13) and Eq.(14). In the work of [11], a lie group integrator of Euclidean motions is shown to be more robust than the Runge-Kutta scheme for large timesteps. Because our work focuses on the falling motion of immersed rigid bodies, we utilize a quite small scale of timestep for the rigid body solver. The Runge-Kutta scheme is efficient enough for our simulation.

7 Results

In this section, we describe the simulation results using the Langevin rigid approach.

In Figure 3 a piece of paper released in air is simulated by our approach. The cross section of the leaf model used in our simulation is elliptical (semi-major axis and minor axis are 4.0 and 1.0 cm respectively). The thickness is set to be 0.01 cm and the density number is 0.8. The Reynolds number (4.3×10^4) is so large that the turbulences can be generated at the

Algorithm 2 Pseudo-code for the runtime computation.

```
Precompute added mass tensors ←Eq.(5)
Initialization of rigid body
Timestep t = 0
while not arrive ground do
    Calculate buoyancy force and torque←Eq.(7)
    Query χ_t and ε_t (Algorithm 1)
    Compute translational velocity v ←Eq.(13)
    Compute angular velocity ω ←Eq.(14)
    Integrate (R, x) ←Eq.(2)
    Render data
    t = t + Δt
end while
```

paper surface. As show in Figure 3, the paper falls down following a helical trajectory which is in compliance with the analysis result in [22]. The motion has the accompanying motion that the paper rotates around the major-axis while falling, which usually happens in real life.

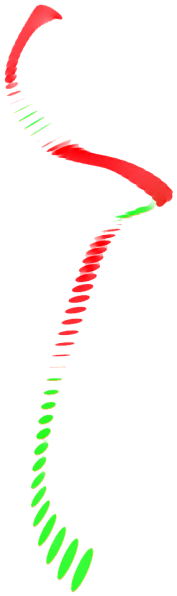

Figure 3: Simulation result of a piece of paper falling in air.

Figure 4 shows a comparison between our simulation and a video of a flying paper airplane. The paper airplane is made by a $8.3 \times 8.3 \times 0.01$ (cm) print paper. The added-mass tensors and moment of inertia of the body depend on the geometries with closed shape, where the fold part of the paper airplane is constructed as volume as shown in the right figure. The simulation begins with an initial velocity of 20 cm/s in the horizontal direction, and the simulated result shows two turning motions (turning front and turning sideways) which are caused by the surrounding airflow. The turning motions are similar to the observation from ground truth in Figure 4.

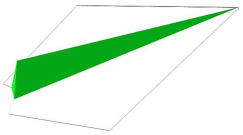

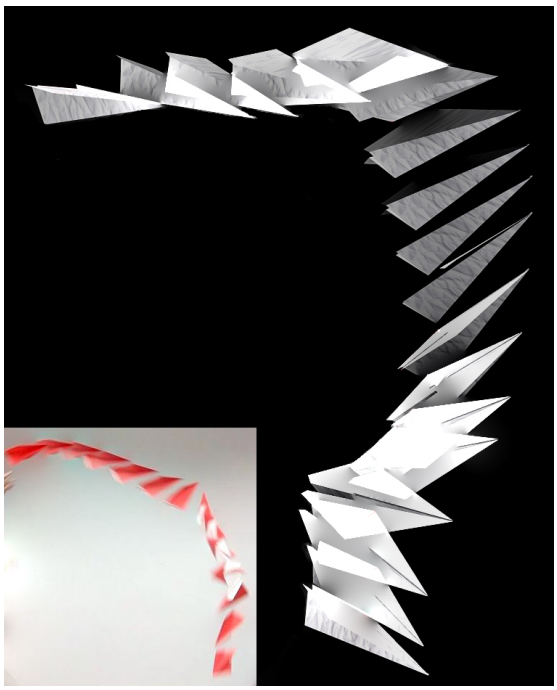

Figure 4: Comparison between the simulation and the ground truth of a flying paper airplane.

Figure 5 shows the discrete frames from the animation of a rubber ellipsoid falling in water, and the time interval is 50 ms. The rubber ellipsoid with semi-principal axes of length 1 cm, 2 cm and 4 cm falls down in a quiescent water flow. A small scale of fluttering motion can be found (Figure 5 (a)) using the simulation method of the previous work [21]. In contrast to the previous work, the coupling between forces and torques due to the surrounding turbulent flow can be indicated properly using our Langevin rigid approach. The oscillations of rigid body in differential directions from falling experiments (Figure 5 (c)) are captured in our simulation, so that our simulation result is more realistic than the previous work.

The precomputation time of added-mass tensors depends on the amount of the body meshes; and the precomputation time of turbulent model depends on the grid solutions of the base flow. In the case of

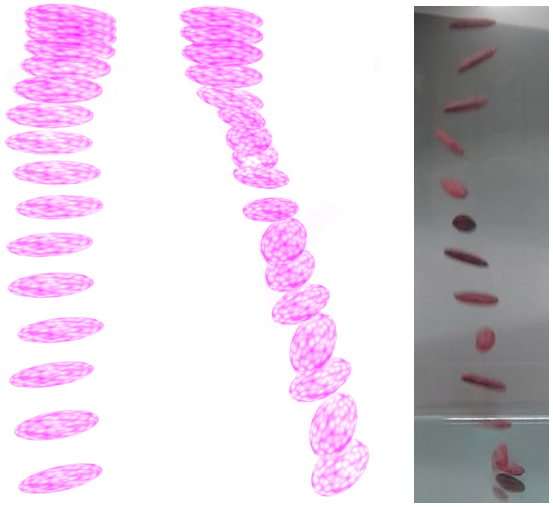

(a) (b) (c)

Figure 5: Comparison between (b) our simulation and (a) the previous work. In (a) only the added-mass tensors are embedded into the Kirchhoff equations, whereas our approach has concerned the force and torque from the surrounding turbulence (b). (c) Ground truth shows oscillations generated in different directions.

1280 meshes and $32 \times 32 \times 8$ MAC grid, the precomputation times are 53 ms and 182 ms, respectively. All simulations were implemented on an Intel Core i7 CPU with 3.20 GHz and 12.0 GB RAM. The simulation time for a single loop of runtime computation is not more than 2.0 ms. As shown in Table 1, the runtime computation time is independent of the body meshes and time step, and it is suitable for real-time simulations.

Table 1: Computation cost of simulation results in runtime.

Rigid bodies	Meshes	Timestep	Average cost
Ellipsoid 1	320	1 ms	1.59 ms
Ellipsoid 1	320	5 ms	1.63 ms
Ellipsoid 1	320	10 ms	1.65 ms
Ellipsoid 2	1280	5 ms	1.71 ms
Piece of paper	1024	5 ms	1.73 ms
Paper airplane	288	5 ms	1.86 ms

8 Conclusion

We presented the Langevin rigid approach for realistic simulations of rigid bodies in viscous, high-Reynolds-number flows. The main strength of the Langevin rigid method lies in combining Kirchhoff equations and Langevin model to represent the chaotic motions of immersed rigid bodies. The method allows a real-time simulation for interactive applications like game.

Limitations exist in the Langevin rigid approach. Because the simulation results are sensitive to the initial conditions, such as released angle and velocities, the appropriate variables should be chosen to meet the ground truth in our simulation results. Some characteristic motions like fluttering and tumbling motions, are not apparently captured by the approximated turbulent model. These limitations can be improved by animation control strategies in future work.

Some fruitful avenues for future work remain. It is possible to extend this Langevin rigid approach to deformable rigid bodies and bubble dynamics. In this paper, the collisions among rigid bodies are not considered, which can be treated as external force and torque in this approach. In addition, the experimental results of falling rigid bodies indicate that six primitive trajectories exist, which can be applied to a motion synthesis approach for simulating the dynamics of immersed bodies [22]. It is promising to combine the Langevin rigid method with the motion synthesis method to achieve more realistic and controllable simulations.

References

[1] C. Batty, F. Bertails, and R. Bridson. A fast variational framework for accurate solid fluid coupling. *ACM Trans. Graph.*, 26(3), July 2007.

[2] M. Becker, H. Tessendorf, and M. Teschner. Direct forcing for lagrangian rigid-fluid coupling. *IEEE Transactions on Visualization and Computer Graphics*, 15(3):493–503, May 2009.

[3] C. E. Brennen. A review of added mass and fluid inertial forces. *NASA STI/Recon Technical Report N*, 82:21535, Jan. 1982.

[4] M. Carlson, P. J. Mucha, and G. Turk. Rigid fluid: animating the interplay between rigid bodies and fluid. *ACM Trans. Graph.*, 23(3):377–384, Aug. 2004.

[5] F. Chen, Y. Zhao, and Z. Yuan. Langevin particle: A self-adaptive lagrangian primitive for flow simulation enhancement. *Computer Graphics Forum*, 30(2):435–444, 2011.

[6] N. Chentanez and M. Müller. Real-time simulation of large bodies of water with small

scale details. In *Proceedings of the 2010 ACM SIGGRAPH/Eurographics Symposium on Computer Animation*, SCA '10, pages 197–206, Aire-la-Ville, Switzerland, Switzerland, 2010. Eurographics Association.

[7] S. Clavet, P. Beaudoin, and P. Poulin. Particle-based viscoelastic fluid simulation. In *Proceedings of the 2005 ACM SIGGRAPH/Eurographics symposium on Computer animation*, SCA '05, pages 219–228, New York, NY, USA, 2005. ACM.

[8] P. Fernandes, P. Ern, F. Risso, and J. Magnaudet. Dynamics of axisymmetric bodies rising along a zigzag path. *Journal of Fluid Mechanics*, 606:209–223, 6 2008.

[9] E. Guendelman, A. Selle, F. Losasso, and R. Fedkiw. Coupling water and smoke to thin deformable and rigid shells. *ACM Trans. Graph.*, 24(3):973–981, July 2005.

[10] M. S. Howe. On the force and moment on a body in an incompressible fluid, with application to rigid bodies and bubbles at high and low reynolds numbers. *The Quarterly Journal of Mechanics and Applied Mathematics*, 48(3):401–426, 1995.

[11] M. Kobilarov, K. Crane, and M. Desbrun. Lie group integrators for animation and control of vehicles. *ACM Trans. Graph.*, 28(2):16:1–16:14, May 2009.

[12] B. E. Launder and B. I. Sharma. Application of the energy-dissipation model of turbulence to the calculation of flow near a spinning disc. *Letters Heat Mass Transfer*, 1:131–137, Dec. 1974.

[13] M. Makino and M. Doi. Brownian Motion of a Particle of General Shape in Newtonian Fluid. *Journal of the Physical Society of Japan*, 73:2739, Oct. 2004.

[14] T. Pfaff, N. Thuerey, J. Cohen, S. Tariq, and M. Gross. Scalable fluid simulation using anisotropic turbulence particles. *ACM Trans. Graph.*, 29(6):174:1–174:8, Dec. 2010.

[15] T. Pfaff, N. Thuerey, A. Selle, and M. Gross. Synthetic turbulence using artificial boundary layers. *ACM Trans. Graph.*, 28(5):121:1–121:10, Dec. 2009.

[16] S. B. Pope. A lagrangian two-time probability density function equation for inhomogeneous turbulent flows. *Physics of Fluids*, 26(12):3448–3450, 1983.

[17] S. B. Pope. Simple models of turbulent flows. *Physics of Fluids*, 23(1):011301, 2011.

[18] B. Solenthaler, J. Schlafli, and R. Pajarola. A unified particle model for fluid solid interactions. *Comput. Animat. Virtual Worlds*, 18(1):69–82, Feb. 2007.

[19] G. E. Uhlenbeck and L. S. Ornstein. On the theory of the brownian motion. *Phys. Rev.*, 36:823–841, Sep 1930.

[20] S. Weissmann and U. Pinkall. Filament-based smoke with vortex shedding and variational reconnection. In *ACM SIGGRAPH 2010 papers*, SIGGRAPH '10, pages 115:1–115:12, New York, NY, USA, 2010. ACM.

[21] S. Weissmann and U. Pinkall. Underwater rigid body dynamics. *ACM Trans. Graph.*, 31(4):104:1–104:7, July 2012.

[22] H. Xie and K. Miyata. Real-time simulation of lightweight rigid bodies. *The Visual Computer*, pages 1–12, 2013.

[23] Z. Yuan, F. Chen, and Y. Zhao. Stochastic modeling of light-weight floating objects. In *Symposium on Interactive 3D Graphics and Games*, I3D '11, pages 213–213, New York, NY, USA, 2011. ACM.